RSC Advances




ROYAL SOCIETY OF CHEMISTRY

www.rsc.org/advances

RSC Advances

RSCPublishing

ARTICLE

# Influence of electron acceptors on the kinetics of metoprolol photocatalytic degradation in $TiO_2$ suspension. A combined experimental and theoretical study§

Cite this: DOI: 10.1039/x0xx00000x

Received 00th January 2014,
Accepted 00th January 2014

DOI: 10.1039/x0xx00000x

www.rsc.org/

S. J. Armaković,[a] S. Armaković,[b] N. L. Finčur,[a] F. Šibul,[a] D. Vione,[c] J. P. Šetrajčić[b] and B. F. Abramović[a]

Metoprolol (MET) belongs to a group of frequently used $\beta_1$-blockers, which often occur in waste waters. The objective of this work was to employ liquid chromatography (LC) and total organic carbon methods to study the photocatalytic degradation of MET in UV irradiated aqueous suspensions of $TiO_2$ (Wackherr's "Oxyde de titane standard" and Degussa P25), in the presence of different electron acceptors such as molecular oxygen, hydrogen peroxide, potassium bromate, and ammonium persulfate. The degradation rates were found to be strongly influenced by the kind of electron acceptor and the type of catalyst. The optimal amount of hydrogen peroxide and potassium bromate was investigated as well. MET photocatalytic degradation was fastest in the presence of $O_2$ and potassium bromate with $TiO_2$ Degussa P25, while mineralization was most efficient in the presence of molecular oxygen alone. In all investigated cases, degradation followed a pseudo-first order kinetics. Reaction intermediates of MET degradation in the presence of different electron acceptors with both catalysts were studied in detail and a number of them were indentified using LC–ESI–MS/MS. The interactions with MET of reactive radical species relevant to this study ( $O_2^{\bullet-}$, $^{\bullet}OH$, $BrO_2^{\bullet}$, and $SO_4^{\bullet-}$ ) were theoretically investigated by means of density functional theory (DFT) computations.

## 1. Introduction

Studies dating more than 30 years ago dealt with photocatalytic reactions, which irrupted into the scientific literature when they were proposed as a suitable tool to promote separation of molecular $H_2$ and molecular $O_2$ from water using solar irradiation.[1,2] Heterogeneous photocatalysis using $TiO_2$ powders has become a subject of increasing interest during the past twenty years, mainly in the field of environmental protection and wastewater decontamination.[3] Photocatalysis in the presence of semiconductors is triggered by the interaction of electrons and holes, generated in a photochemically activated solid, with the surrounding medium. Activation is the consequence of light absorption: the irradiation of the photocatalytic material with sufficient energy leads to the formation of holes ($h^+$) in the valence band and electrons ($e^-$) in the conduction band.

[a] Department of Chemistry, Biochemistry and Environmental Protection, Faculty of Sciences, University of Novi Sad, Trg Dositeja Obradovića 3, 21000 Novi Sad, Serbia
*E-mail: biljana.abramovic@dh.uns.ac.rs; Tel.: +381 214852753; Fax: +381 21454065.*
[b] Department of Physics, Faculty of Sciences, University of Novi Sad, Trg Dositeja Obradovića 4, 21000 Novi Sad, Serbia
[c] Dipartimento di Chimica, Università di Torino, Via Pietro Giuria 5, 10125 Torino, Italy
§ Electronic supplementary information (ESI) available: Influence of electron acceptors on the kinetics of metoprolol photocatalytic degradation in $TiO_2$ suspension. A combined experimental and theoretical study.

The two species can either recombine or participate in reductive and oxidative reactions that lead to the decomposition of contaminants.[4]

The $h^+$ can either directly oxidize pollutants, or oxidize water (preferably the $OH^-$ groups adsorbed on the solid surface) to produce $^{\bullet}OH$. In contrast, $e^-$ reduces surface-adsorbed $O_2$. The oxidative and reductive reaction steps taking place with the irradiated photocatalyst ($TiO_2$) are expressed as follows:[5–8]

$$TiO_2 + h\nu \rightarrow e^- + h^+ \quad (1)$$

$$h^+ + \text{organic compound} \rightarrow CO_2 + H_2O + \text{inorganic ions} \quad (2)$$

$$H_2O + h^+ \rightarrow {}^{\bullet}OH + H^+ \quad (3)$$

$$O_2 + e^- \rightarrow O_2^{\bullet-} \quad (4)$$

A practical problem in using $TiO_2$ as a photocatalyst is the energy waste due to the $e^-$–$h^+$ recombination, which results in lower degradation efficiency. The prevention of recombination is thus very important, and it can be achieved by adding proper electron acceptors. In the simplest systems, in aerated solution, molecular $O_2$ acts as electron acceptor to prevent $e^-$–$h^+$ recombination.[9] Additional oxidants, such as $H_2O_2$, $S_2O_8^{2-}$, and $BrO_3^-$, can act as electron acceptors to enhance the photodegradation efficiency. These electron acceptors can have several effects including: (I) avoidance of $e^-$–$h^+$ recombination because of scavenging of conduction-band electrons; (II) increase of the concentration of $^{\bullet}OH$ and (III) production of other oxidizing species that can enhance the oxidation rate of the substrate and of its intermediate compounds.[10]

By employing computer simulations within the framework of the density functional theory (DFT), it is possible to gain insight into the changes of the investigated structures as a consequence of the presence of other molecules in the system.[11,12] The information thus obtained is very important to further understand the degradation mechanisms of the investigated compounds.[13,14]

Fukui functions and Fukui indices are often used as local quantum-molecular descriptors. Fukui functions describe the changes in the molecular electron density as a consequence of the addition or removal of charge, while Fukui indices represent scalar values for each atom. Fukui functions are visualized as iso-surfaces, and larger Fukui values indicate higher reactivity.[15,16] It should be emphasized that values of Fukui functions are sensitive to changes in basis sets and population analysis. Therefore, one shouldn't use these values as absolute but rather as comparative parameters.

The molecular electrostatic potential (MEP) is related to the charge distribution and it is a very useful descriptor to determine potential sites prone to electrophilic attack and nucleophilic reactions.[14,17,18] In the field of pollutant degradation, MEP enables the localization of parts of a molecule that are prone to various types of attacks, also giving information on how molecules interact with other molecules or radicals. The MEP (hereafter indicated as *V(r)*), when neglecting polarization and nuclear rearrangement effects due to the presence of a unit test charge at the distance *r*, is given as follows:

$$V(\vec{r}) = \sum \frac{Z_A}{|R_A - \vec{r}|} - \int \frac{\rho(\vec{r}')}{|\vec{r}' - \vec{r}|} d\vec{r} \qquad (5)$$

where the summation runs over all nuclei A with charge $Z_A$ and coordinate $R_A$, while $\rho(r')$ is the electron density of the molecule. $V(r)$ represents the potential exerted at the coordinate $r$ by the nuclei and the electrons. The sign of $V(r)$ at any point depends on whether the effects of the nuclei or the electrons are dominant.[19,20]

Natural bond order (NBO) can be used for efficient investigation of intra- and inter-molecular bonding and interactions. It is a convenient basis for the investigation of charge transfer or conjugative interactions in molecular systems.[21–23] NBO analysis is carried out by examining all possible interactions between 'filled' (donor) NBOs and 'empty' (acceptor) NBOs, estimating their energetic importance by 2nd-order perturbation theory. In this way one obtains the energies of delocalization of electrons from filled NBOs into empty NBOs, *e.g.* stabilization energies gained by donation from the donor NBO to the acceptor NBO. For each donor NBO (*i*) and acceptor NBO (*j*), the stabilization energy associated with $i \rightarrow j$ delocalization can be estimated on the basis of the second-order perturbation theory:[24–26]

$$E(2) = \Delta E_{ij} = q_i \frac{F(i,j)^2}{\varepsilon_i \varepsilon_j} \qquad (6)$$

where $q_i$ is the donor orbital occupancy, $\varepsilon_i$, $\varepsilon_j$ are diagonal elements (orbital energies) and $F_{(i,j)}$ is the off-diagonal NBO Fock matrix element.

Metoprolol (MET) is a selective $\beta_1$-blocker of the cardiac adrenergic receptors.[27] Due to the frequent use, MET is present in sewage waters, in rivers from Netherlands (25–100 ng $L^{-1}$),[28] Poland (51–155 ng $L^{-1}$),[29] UK (7–11 ng $L^{-1}$)[30], Sweden (60–70 ng $L^{-1}$),[30] and Germany (exceeding 1000 ng $L^{-1}$).[31]

Previous work has shown that the rate of MET photocatalytic degradation tended to a plateau at about 0.5–1.0 mM initial concentration of the substrate, and that photodegradation was most efficient at a photocatalyst loading of 1.0 mg $mL^{-1}$.[13] The aim of this work was to compare the kinetics of photodegradation of MET, sensitized by $TiO_2$ Wackherr or Degussa P25 in aqueous suspension under the same experimental conditions, in the presence of different electron acceptors ($O_2$, $H_2O_2$, $S_2O_8^{2-}$, and $BrO_3^-$). To monitor MET removal and mineralization, liquid chromatography (LC) and total organic carbon (TOC) analysis were used, respectively. An attempt has also been made to identify the intermediates formed during the photooxidation of MET in the presence of different electron acceptors with both catalysts, and a number of them were indentified using LC–ESI–MS/MS. Employing DFT computations, the interactions of radical species ($O_2^{\bullet-}$, $^{\bullet}OH$, $BrO_2^{\bullet}$, and $SO_4^{\bullet-}$) with MET and their possible effects on its degradation were investigated from the aspect of structural considerations, charge distribution, NBO analysis, Fukui functions and Fukui indices.

## 2. Materials and methods

### 2.1. Chemicals and solutions

All chemicals were of reagent grade and were used without further purification. The drug (±)-Metoprolol(+)-tartrate salt (Sigma-Aldrich) was used as received (≥99% purity); 85% $H_3PO_4$ was purchased from Lachema, Neratovice; acetonitrile (ACN) was a product of J.T. Baker. Other chemicals were as follows: 30% $H_2O_2$ from Sigma-Aldrich; $KBrO_3$ and $(NH_4)_2S_2O_8$ from Merck. All solutions were made using doubly distilled water. The used catalysts were $TiO_2$ Degussa P25 (75% anatase and 25% rutile, surface area 50 ± 1.0 $m^2$ $g^{-1}$, crystallite size about 20 nm, non-porous) and $TiO_2$ Wackherr's "Oxyde de titane standard" (100% anatase, surface area 8.5±1.0 $m^2$ $g^{-1}$, crystallite size 300 nm, hereafter "$TiO_2$ Wackherr"), produced by the sulfate process.[32]

### 2.2. Photodegradation procedures

Photocatalytic degradation was carried out in a cell made of Pyrex glass (total volume of ca. 40 mL, liquid layer thickness 35 mm), with a plain window on which the light beam was focused. The cell was equipped with a magnetic stirring bar and a water circulating jacket. A 125 W high-pressure mercury lamp (Philips, HPL-N, emission bands in the UV region at 304, 314, 335 and 365 nm, with maximum emission at 365 nm) together with an appropriate concave mirror was used as the radiation source. The output of the mercury lamp was calculated to be ca. $8.8 \times 10^{-9}$ Einstein $mL^{-1}$ $min^{-1}$ (potassium ferrioxalate actinometry).

Experiments were performed using 20 mL of 0.05 mM MET containing 1.0 mg $mL^{-1}$ of $TiO_2$ (Wackherr or Degussa P25), except for the study of direct photolysis. The aqueous suspension of $TiO_2$ was sonicated (50 Hz) in the dark for 15 min before irradiation, in order to uniformly disperse the photocatalyst particles and to attain adsorption equilibrium. Before irradiation, the suspension thus obtained was thermostated at 25±0.5 ºC in a stream of $O_2$ (3.0 mL $min^{-1}$), except for a control run in the absence of electron acceptors when $N_2$ was bubbled (3.0 mL $min^{-1}$) to remove dissolved



 

oxygen. During irradiation, the mixture was stirred at a constant rate under continuous gas flow. All experiments were performed at the natural pH which changed during the photodegradation, from pH 7 to pH 4 in the case of $TiO_2$ Wackherr and from pH 7 to pH 5 in the case of Degussa P25. In the investigation of the influence of electron acceptors, apart from constant $O_2$ bubbling, solutions of $H_2O_2$, $KBrO_3$ or $(NH_4)_2S_2O_8$ (at typical 3.0 mM initial concentration) were added to the MET solution.

### 2.3. Analytical procedures

The photodegradation of MET was monitored by liquid chromatography–photodiode array detection (LC–PDA). To do so, aliquots of 0.30 mL were taken from the reaction mixture at the beginning of the experiment and at regular time intervals. Aliquot sampling caused a maximum volume variation of ca. 10% in the reaction mixture. The suspensions were filtered through Millipore (Millex-GV, 0.22 μm) membrane filters to eliminate the photocatalyst. Lack of adsorption of MET on the filters was preliminarily checked. Afterwards, a 10-μL sample was injected and analyzed using a Shimadzu UFLC–PDA, equipped with an Eclipse XDB-C18 column (150 mm × 4.6 mm i.d., particle size 5 μm, 25 °C). The UV/vis PDA detector was set at 225 nm (wavelength of MET maximum absorption), as well as at 210, 260, 270 and 280 nm for the monitoring of the intermediates. The mobile phase (flow rate 0.8 mL $min^{-1}$) was a mixture of ACN and water (the latter acidified with 0.1% $H_3PO_4$), with the following gradient: 15% ACN at 0 min, which was increased to 30% ACN in 5 min, after which 30% ACN was constant for 5 min; post time was 3 min. The retention time for MET was 6.0 ± 0.1 min. Reproducibility of repeated runs was around 3–10%.

Concerning TOC analysis, 10 mL aliquots of the reaction mixture were taken at regular time intervals, diluted to 25 mL and analyzed after filtration on an Elementar Liqui TOC II analyzer, according to Standard US 120 EPA Method 9060A. For the LC–ESI–MS/MS evaluation of intermediates after 10 min irradiations, 100-μL samples were analyzed on an Agilent Technologies 1200 series LC with Agilent Technologies 6410A series electrospray ionization triple-quadrupole MS/MS, using Agilent Technologies Zorbax XDB-C18 column (50 × 4.6 mm i.d., particle size 1.8 μm, 40°C). The mobile phase (flow rate 0.5 mL $min^{-1}$) consisted of 0.05% aqueous formic acid and MeOH (gradient, 0 min 20% MeOH, 10 min 60% MeOH, 12 min 100% MeOH, post-time 3 min). Analytes were ionized using the electrospray ion source, a capillary voltage of 4.0 kV and with nitrogen as the drying gas (temperature 350°C, flow 10 L $min^{-1}$) and nebulizer gas (45 psi). High-purity nitrogen was used as the collision gas. Full scan mode (*m/z* range 50–800, scan time 100 ms, fragmentor voltage 100 V) in positive ion mode was used to select precursor ions for the starting compound and each degradation intermediate, as well as to examine isotopic peak distribution. Then, the product ion scan $MS^2$ mode (fragmentor voltage 135 V, scan time 200 ms, collision energy 10–40 V in increments of 10 V) was used to elucidate the structure of each degradation intermediate.

### 2.4. Computational details

All DFT calculations were carried out using the Gaussian 03 software package,[33] except for Fukui functions and Fukui indices that were calculated at the same level of theory using Jaguar, version 8.4,[34] as implemented in the Schrödinger Materials Suite, release 2014-2. For the purpose of NBO analysis, it was used the NBO 3.0 program as implemented in Gaussian 03. For all systems, calculations were performed employing the B3LYP exchange and correlation functional with 6-31 G+(d) basis set.[35] Two stages took place for all configurations. Firstly, equilibrium geometry of the investigated systems was located using default convergence criteria and, secondly, the harmonic vibrational spectrum was checked to assure that the true minimum of potential energy, characterized by positive frequencies, was located.

In this work we investigated five systems: MET, MET/$O_2^{\bullet-}$, MET/$O_2^{\bullet-}$/$^{\bullet}OH$, MET/$O_2^{\bullet-}$/$BrO_2^{\bullet}$, and MET/$O_2^{\bullet-}$/$SO_4^{\bullet-}$. To make the simulations more realistic, solvent effects of water were taken into account using the default Polarizable Continuum Model (PCM). Initially, in all cases $O_2^{\bullet-}$ was placed above the hydroxyl group located at the tail of MET, while $^{\bullet}OH$, $BrO_2^{\bullet}$ and $SO_4^{\bullet-}$ were placed above the aromatic ring.

Interesting sites containing a significant amount of charges were located through MEP surfaces, which were obtained using Molekel after geometry optimization and frequency check.[36]

## 3. Results and discussion

### 3.1. Effect of electron acceptors

Apart from $O_2$, which is the most frequently applied electron acceptor, in this work we also investigated the influence of $H_2O_2$, $BrO_3^-$, and $S_2O_8^{2-}$. These compounds operate as $e^-$ scavengers and should be able to prevent $e^-$–$h^+$ recombination, thereby enhancing the formation of $^{\bullet}OH$ and other reactive species.[5,6] However, compounds such as $H_2O_2$ are also able to scavenge the photogenerated transients.[37]

Fig. 1 and Table 1 show the time trend and degradation kinetics of MET, upon irradiation in the presence of $TiO_2$ (Wackherr, 1a, and Degussa P25, 1b) and several electron acceptors. In all investigated cases, the degradation process followed a pseudo-first order kinetics. Note that the role of $O_2$ as electron acceptor was investigated by comparing the system in air (blue triangles) with the one in which oxygen was bubbled to create an $O_2$ atmosphere (purple stars; in such a system, the concentration of both gas-phase and dissolved $O_2$ is expected to be ~5 times higher than in the case of air equilibrium). For further comparison, the behaviour of the deoxygenated system ($N_2$ bubbling, pink triangles) was also studied.

As expected, all the studied electron acceptors increased the efficiency of MET photocatalytic removal. It was determined that the influence of electron acceptors on the efficiency of degradation followed the order: $O_2/H_2O_2 > O_2 \approx O_2/S_2O_8^{2-} \approx O_2/BrO_3^-$ using $TiO_2$ Wackherr, and $O_2/BrO_3^- > O_2/H_2O_2 > O_2/S_2O_8^{2-} > O_2$ using Degussa P25 (Fig. 1, Table 1). The added oxidants ($H_2O_2$, $BrO_3^-$, $S_2O_8^{2-}$) did not cause MET transformation in the dark.

Moreover, MET degradation using $TiO_2$ under $N_2$ atmosphere was very slow, and only marginally faster compared to the direct photolysis (MET irradiation in air without $TiO_2$). As reported in Fig. 1 and Table 1, a considerable enhancement of MET degradation was observed, with irradiated $TiO_2$, in air compared to $N_2$ atmosphere: the increase of the pseudo-first order rate constant $k'$ was around 7 times with $TiO_2$ Wackherr and around 12 times with Degussa P25.

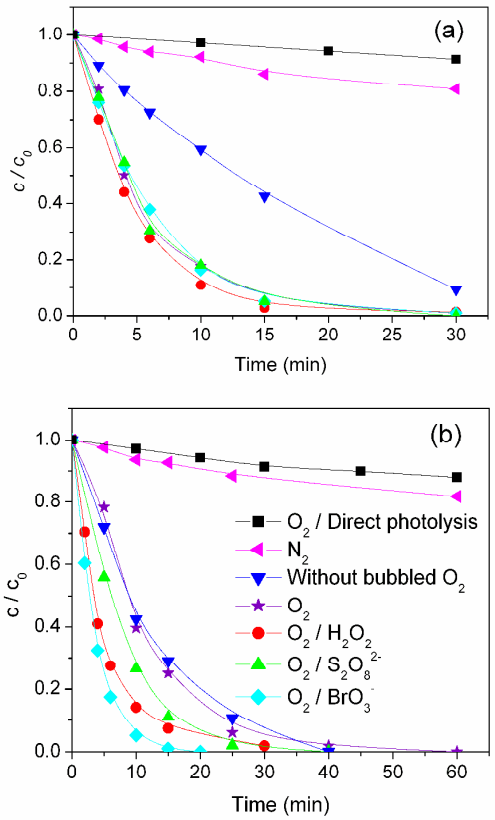


Fig. 1 Kinetics of the photolytic/photocatalytic removal of MET using $TiO_2$ Wackherr (a) and Degussa P25 (b) under UV irradiation, in the absence/presence of different electron acceptors.

Table 1. Values of the first-order decay constant, k', for the photolytic/ photocatalytic removal of MET (initial concentration 0.05 mM) using $TiO_2$ (where applicable) and UV radiation, as a function of the absence/presence of different electron acceptors

| | k' ($min^{-1}$)* | |
|---|---|---|
| Direct photolysis | 0.0029 | |
| | $TiO_2$ Wackherr | Degussa P25 |
| $N_2$ | 0.008 | 0.007 |
| Without bubbled $O_2$ | 0.054 | 0.086 |
| $O_2$ | 0.184 | 0.092 |
| $O_2/H_2O_2$ | 0.224 | 0.199 |
| $O_2/ BrO_3^-$ | 0.172 | 0.299 |
| $O_2/ S_2O_8^{2-}$ | 0.180 | 0.133 |

* k' determined after 10 min of irradiation.

In all cases, correlation coefficient was higher than 0.95

Moreover, while MET degradation with Degussa P25 was little influenced by a further increase of the oxygen concentration (compare the runs with and without bubbled $O_2$), a further significant increase of the MET rate constant (over three times) was observed with $TiO_2$ Wackherr. Interestingly, in the case of $TiO_2$ Wackherr the degradation of MET did not undergo a further important enhancement upon addition of other $e^-$ scavengers. In contrast, with Degussa P25 the additional effect of the scavengers was substantial. The differences between the two photocatalysts may be connected with the different surface area (much larger for Degussa P25) and different crystal structure (presence of the rutile phase in Degussa P25). These issues could lead to differences in the interaction of $O_2$ and other $e^-$ scavengers with the photocatalyst surface. In the case of $TiO_2$ Wackherr, it appears that $O_2$ bubbling already brought the reaction to its optimum and that any further enhancement was difficult. The situation was very different for Degussa P25.

As far as the role of $O_2$ as electron acceptor is concerned, photoelectrons can be captured by $O_2$ to produce $O_2^{\bullet-}$, $H_2O_2$ (reactions 4, 7, and 8) and then eventually hydroxyl radicals (reactions 9-11):[8,10,38]

$$O_2^{\bullet-} + H^+ \rightarrow HO_2^{\bullet} \quad (7)$$

$$2HO_2^{\bullet} \rightarrow H_2O_2 + O_2 \quad (8)$$

$$H_2O_2 + h\nu \rightarrow 2^{\bullet}OH \quad (9)$$

$$H_2O_2 + e^- \rightarrow {}^{\bullet}OH + OH^- \quad (10)$$

$$H_2O_2 + O_2^{\bullet-} \rightarrow {}^{\bullet}OH + OH^- + O_2 \quad (11)$$

When comparing the systems $O_2$ and $O_2/H_2O_2$ (oxygen bubbling in both cases, reported as purple stars and red circles, respectively, in Fig. 1), one can notice a small acceleration (by a factor of 1.2) caused by $H_2O_2$ addition in the case of $TiO_2$ Wackherr, and a more marked $H_2O_2$ effect (2.2 times) with Degussa P25. Despite the more important role of $H_2O_2$, MET degradation with Degussa P25 and $O_2/H_2O_2$ was still a bit slower compared to $TiO_2$ Wackherr with otherwise identical conditions. The fact that a photocatalyst with lower surface area ($TiO_2$ Wackherr) could induce faster MET degradation compared with Degussa P25 is most likely accounted for by lower radiation scattering, which allows a better use of the incoming photons.[13]

The increase of MET degradation rate upon addition of $H_2O_2$ to Degussa P25 (Table 1) was likely due to increased generation of $^{\bullet}OH$. Indeed, $H_2O_2$ can enhance $^{\bullet}OH$ production through the following pathways: (I) direct photolysis of $H_2O_2$ under UV irradiation (reaction 9); (II) reaction between $H_2O_2$ and $e^-$: $H_2O_2$ is a more effective electron acceptor than oxygen because its reaction with $e^-$ yields $^{\bullet}OH$ and $OH^-$ (reaction 10), while the corresponding process with $O_2$ produces the weaker oxidant $O_2^{\bullet-}$ (reaction 4); (III) reaction with $O_2^{\bullet-}$, also yielding $^{\bullet}OH$ (reaction 11).[8,10,38]

In the presence of Degussa P25, the $O_2/ BrO_3^-$ system was the most efficient for the degradation of MET. In contrast, the addition of $BrO_3^-$ did not have an important effect on MET degradation with $TiO_2$ Wackherr. When operational, the enhancement of photodegradation efficiency would likely be a consequence of the reaction between $BrO_3^-$ and conduction-band electrons. A first effect is the inhibition of $e^-$–$h^+$ recombination, which prolongs the life time of the photogenerated holes. One should additionally consider the formation of the reactive species $BrO_2^{\bullet}$ (reaction 12).[38,39] The possible role of $BrO_2^{\bullet}$ in MET degradation was investigated with DFT methods (*vide infra*).

$$BrO_3^- + 2\,H^+ + 2\,e^- \rightarrow BrO_2^{\bullet} + H_2O \quad (12)$$

The addition of persulfate to the $O_2$-bubbling system (to obtain $O_2/ S_2O_8^{2-}$) had a limited enhancement effect in the case of Degussa P25 (1.4 times) and practically no effect with $TiO_2$ Wackherr. The reaction (13) between $S_2O_8^{2-}$ and $e^-$ yields the

strong oxidant $SO_4^{\bullet-}$, but $SO_4^{2-}$ is also formed and it can act as a hole scavenger (reaction (14)).[10,38] The trade-off between $h^+$ and $SO_4^{\bullet-}$ could result into a limited enhancement effect, or even into no effect.[10]

$$S_2O_8^{2-} + e^- \rightarrow SO_4^{2-} + SO_4^{\bullet-} \quad (13)$$

$$SO_4^{2-} + h^+ \rightarrow SO_4^{\bullet-} \quad (14)$$

Another issue is that sulfate, formed in reaction (13), can be adsorbed on the $TiO_2$ surface and decrease the photocatalytic activity of the oxide.[10] Since $S_2O_8^{2-}$ turned out to be quite ineffective as electron acceptor in the removal of MET, it was not subjected to further investigation. The very low interaction between $SO_4^{\bullet-}$ and MET, compared to other systems, was confirmed through theoretical analysis as well (*vide infra*).

The results reported, and in particular the much faster transformation of MET with $O_2$ compared to $N_2$ bubbling, highlight the importance of electron acceptors in the degradation process. The addition of further electron acceptors may enhance degradation, but the reaction pathways are probably modified as well. Fig. 2 reports chromatograms obtained using $TiO_2$ Wackherr and Degussa P25 in the presence of the studied electron acceptors, showing that the occurrence of certain intermediates (represented by unassigned peaks) significantly depended on the applied electron acceptor and catalyst. Moreover, according to literature data,[10,38,40,41] it is suggested that the application of an optimal concentration of electron acceptors is of great importance to achieve the maximum removal of organic compounds from the system. For this reason, the effects of the acceptor concentrations were studied in this case as well.

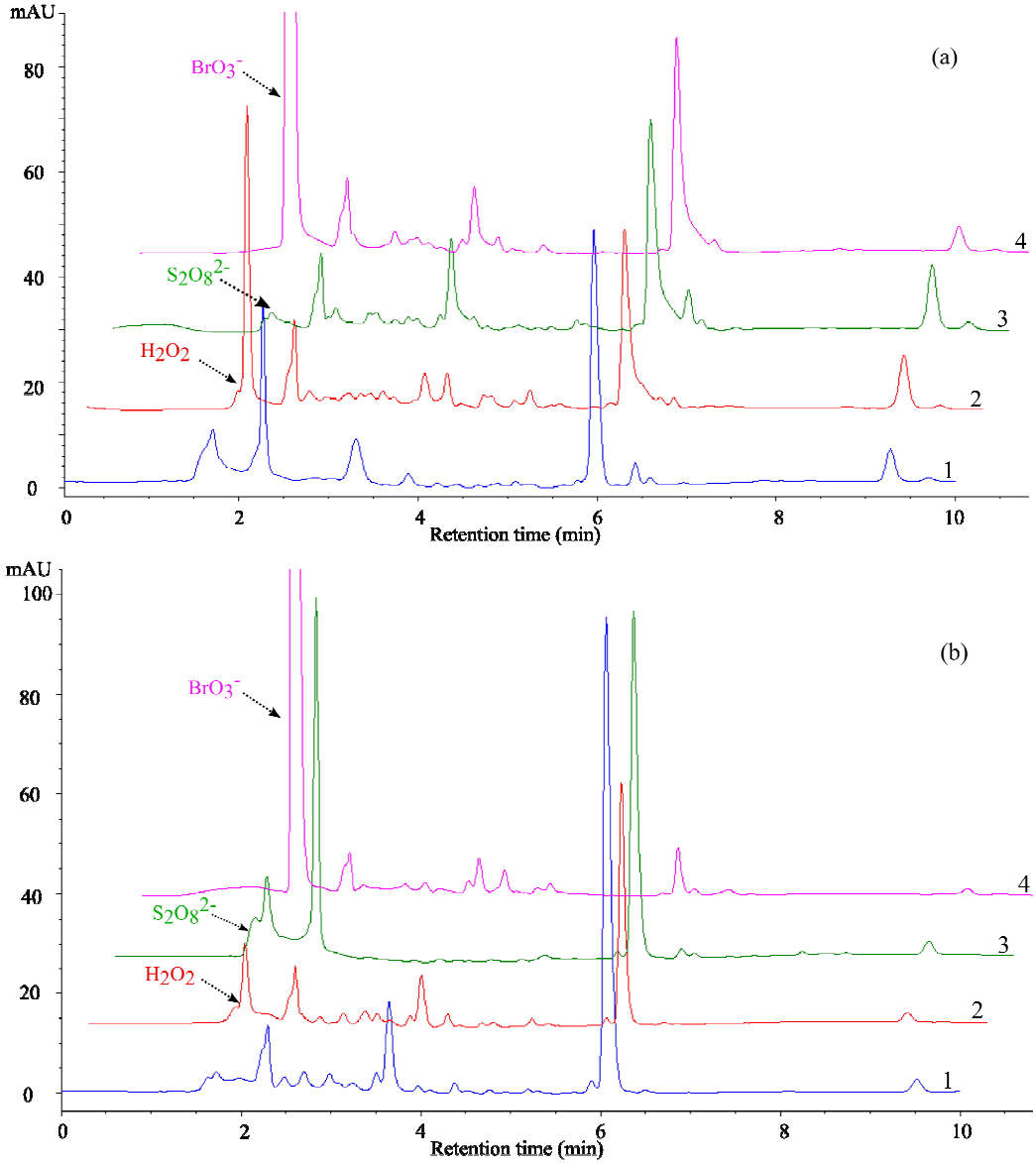


Fig. 2 Chromatograms obtained after 10 min of MET exposure to UV irradiation in the presence of $TiO_2$ Wackherr (a) and Degussa P25 (b), using different electron acceptors (1: $O_2$ 2: $H_2O_2$; 3: $S_2O_8^{2-}$; 4: $BrO_3^-$). $\lambda_{det}$ = 225 nm

RSC Advances RSCPublishing

ARTICLE

### 3.2. Effect of the initial concentration of hydrogen peroxide

The influence of the concentration of $H_2O_2$ on the efficiency of MET removal was investigated in the range of 1.0 to 5.0 mM (Fig. 3). For both Degussa P25 and $TiO_2$ Wackherr, the optimal concentration of $H_2O_2$ was 3 mM. Under such conditions, after 10 min irradiation of the $O_2/H_2O_2$ system, the degradation of MET reached 89% with $TiO_2$ Wackherr and 86% with Degussa P25 (Fig. 3).

The presence of $H_2O_2$ at concentration values above 3 mM resulted in lower MET degradation compared to the optimal conditions. The most likely reason is that $H_2O_2$ acts as an $^{\bullet}OH$ scavenger, generating the much less reactive hydroperoxyl/superoxide radicals ($HO_2^{\bullet}/O_2^{\bullet-}$, reaction 15). Moreover, $HO_2^{\bullet}$ can further react with $^{\bullet}OH$ to form oxygen and water, which are not directly involved into MET degradation (reaction 16).[10,40]

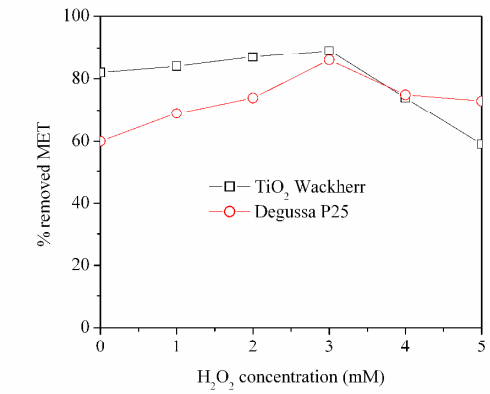


Fig. 3 Effect of the initial concentration of $H_2O_2$ on MET removal using $O_2/UV/TiO_2$ for the first 10 min irradiation.

$$H_2O_2 + {}^{\bullet}OH \rightarrow HO_2^{\bullet} + H_2O \text{ (or } O_2^{\bullet-} + H^+ + H_2O) \quad (15)$$

$$HO_2^{\bullet} + {}^{\bullet}OH \rightarrow O_2 + H_2O \quad (16)$$

Additionally, $H_2O_2$ at elevated concentration could react with $TiO_2$ to form peroxo compounds, which are detrimental to the photocatalytic action.[42]

### 3.3. Effect of the initial concentration of potassium bromate

Fig. 4 reports the MET degradation efficiency in the presence of different initial concentrations of $BrO_3^-$. In the case of $TiO_2$ Wackherr, as already discussed, the bromate effect was very limited. In contrast, Degussa P25 showed a degradation increase that quickly tended to a plateau. In the latter case the most effective MET degradation was observed for 3 mM bromate, but very little difference could be detected in the 3-5 mM $BrO_3^-$ concentration range. While $e^-$ scavenging and a potential involvement of $BrO_2^{\bullet}$ (formed in reaction (12)) could possibly enhance degradation, at elevated $BrO_3^-$ levels the system reactivity could be limited by the formation of bromide (reaction (17)). The latter could both adsorb on the photocatalyst surface and be involved in $h^+$ and $^{\bullet}OH$ scavenging.[10,38,41,43,44]

$$BrO_3^- + 6H^+ + 6\,e^- \rightarrow [\,BrO_2^-, HOBr] \rightarrow Br^- + 3H_2O \quad (17)$$

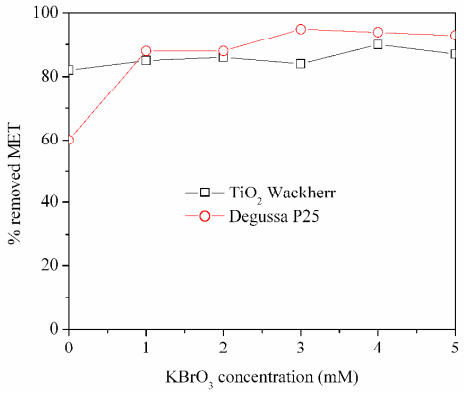


Fig. 4 Effect of the initial concentration of $BrO_3^-$ on MET removal using $O_2/UV/TiO_2$ for the first 10 min of irradiation.

In the studied systems the electron acceptors are expected to inhibit the $e^-$–$h^+$ recombination processes, but they could have additional effects (e.g. production of reactive species by photolysis, such as $^{\bullet}OH$ from $H_2O_2$, see reaction (9)). These effects can be highlighted in the absence of $TiO_2$. For this reason, MET was irradiated alone and in the presence of $O_2/H_2O_2$ and $O_2/BrO_3^-$, without $TiO_2$ (Fig. 5). The degradation of MET was considerably slower compared to photocatalytic conditions, but in the presence of $H_2O_2$ around 50% of MET was removed from the system after 60 minutes irradiation. In this case, acceleration of degradation compared to MET direct photolysis would probably be accounted for by $^{\bullet}OH$, generated by $H_2O_2$ irradiation. Indeed, the hydroxyl radical reacts rapidly and non-selectively with most organic compounds, either by H-abstraction or by addition to C=C unsaturated bonds.[45] Although slower compared to MET photocatalytic degradation, the use of $H_2O_2$ under irradiation could be attractive due to its simplicity.

Some enhancement of MET degradation was also observed in the presence of irradiated bromate, in particular at longer irradiation times (> 30 min), in agreement with literature reports.[46]

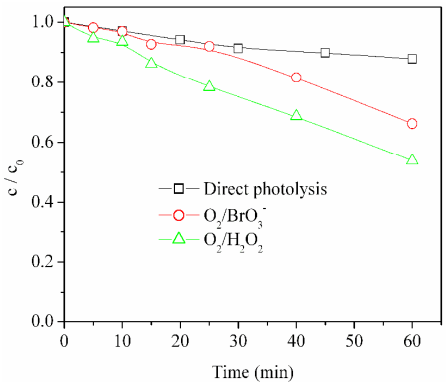


Fig. 5 Kinetics of the direct and indirect photolysis of MET under UV irradiation in the presence of $O_2$, $O_2$/ $BrO_3^-$ and $O_2/H_2O_2$

### 3.4. Evaluation of the degree of mineralization

#### 3.4.1 Systems with hydrogen peroxide

$H_2O_2$ was poorly retained by the analytical column, but its considerable absorption at 225 nm allowed a rough estimation of its concentration to be derived from the chromatograms. By so doing, a considerable decrease of $H_2O_2$ concentration under photocatalytic conditions could be highlighted with both $TiO_2$ Wackherr and Degussa P25. Note that such an approach could overestimate $H_2O_2$ in the degraded systems, because of the possible interference by other poorly retained compounds. Therefore, the extent of $H_2O_2$ degradation could be underestimated. The chromatograms reported in Fig. 6 also show that the variety and the amount of intermediates depended on the type of photocatalyst. We made similar conclusions also in our previous works, where degradation mechanism[13] and toxicity of investigated systems[47] were studied in details. Interestingly, most intermediates formed with both photocatalysts had lower retention times compared to MET: they mainly consisted of ring-hydroxylated compounds and of derivatives arising from oxidative cleavage of the shorter lateral chain of MET (that containing the methoxy group).[13] The mixture of intermediates with Degussa P25 was considerably more toxic than that obtained with $TiO_2$ Wackherr.[47]

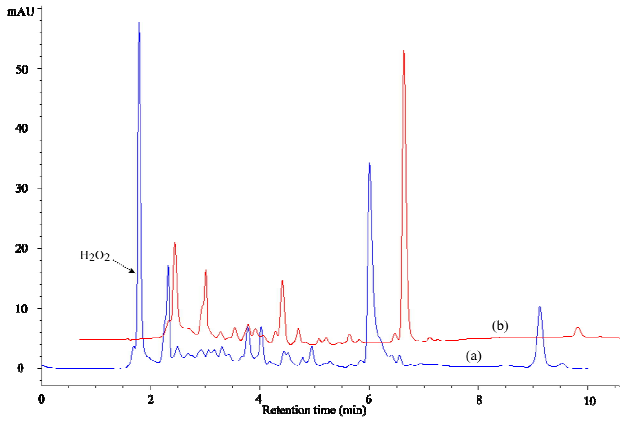


Fig. 6. Chromatograms obtained after 10 min of MET irradiation in the presence of $TiO_2$ Wackherr (a) and Degussa P25 (b): $O_2/H_2O_2$ system in both cases ($O_2$ bubbling, 3 mM $H_2O_2$), $\lambda_{det}$ = 225 nm

Therefore, the ability of the systems to achieve MET mineralization is particularly important in the case of the Degussa P25 photocatalyst. Further experimental results obtained in the present work indicate that the adsorption of MET on the catalysts doesn't differ more than 10%, which leads to conclusion that the adsorption of the investigated compound doesn't have significant influence on the efficiency of photocatalytic degradation. As far as mineralization is concerned, soon after complete removal of MET from the system, 88% of organic compounds (measured as organic carbon) were still present with $TiO_2$ Wackherr in the absence of $H_2O_2$, and even 94% (that is, only 6% mineralization) with 3 mM $H_2O_2$ (Fig. 7a). The degree of mineralization after MET disappearance was significantly higher using Degussa P25, which gave 33% residual organic carbon without $H_2O_2$ and 72% with $H_2O_2$ (Fig. 7b). Photonic efficiencies[48] calculated from data obtained for 60 min of mineralization of MET in the presence of $TiO_2$ Wackherr and Degussa P25 without $H_2O_2$ were 0.068%, and 0.223%, respectively. Also, for the systems $TiO_2$ Wackherr and Degussa P25 in the presence of $H_2O_2$, the photonic efficiency was 0.012% and 0.066%, respectively. The better performance of Degussa P25 toward mineralization, compared to $TiO_2$ Wackherr, could be accounted for by its higher surface area. Indeed, a photocatalyst with low surface area, such as $TiO_2$ Wackherr, could undergo surface poisoning by the degradation intermediates.[13] As an alternative or in addition, the mineralization of MET could be connected with reactions involving $h^+$. The latter are favoured in the presence of Degussa P25 compared with $TiO_2$ Wackherr, which induces $^{\bullet}OH$ reactions to a higher extent.[13] This issue would be consistent with the previously discussed finding (Fig. 2) that different chromatographic peaks, corresponding to different intermediates, could be detected with the two photocatalysts.

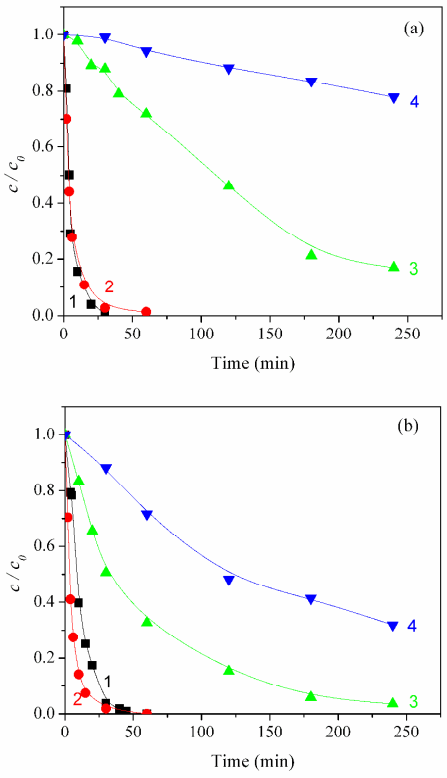


Fig. 7. Kinetics of photocatalytic degradation of MET under UV irradiation and $O_2$ bubbling, in the presence of $TiO_2$ Wackherr (a) and Degussa P25 (b): (1) MET trend, no $H_2O_2$; (2) MET trend, 3 mM $H_2O_2$; (3) TOC trend, no $H_2O_2$; (4) TOC trend, 3 mM $H_2O_2$.

With both $TiO_2$ types, mineralization further increased up to the longest irradiation time (4 h). However, while $H_2O_2$ enhanced MET degradation (at least with Degussa P25), it slowed down mineralization with both photocatalysts. If the above hypothesis concerning $h^+$ vs. $^{\bullet}OH$ is correct, the addition of $H_2O_2$ would shift the system reactivity towards the hydroxyl radical and the inhibition of mineralization would be automatically explained.

### 3.4.2 Systems with potassium bromate

In a similar way as $H_2O_2$, bromate was poorly retained by the analytical column but it could be detected due to significant radiation absorption at 225 nm. An approximate assessment of $BrO_3^-$ concentration could thus be obtained from the chromatograms, similarly to $H_2O_2$ and with the same limitations. Contrary to $H_2O_2$, for which clear evidence of a concentration decrease under photocatalytic conditions was obtained, no evidence was available from the chromatograms of a change in bromate concentration. Fig. 8 shows the chromatograms obtained after 10 minutes of MET degradation in the system $O_2/BrO_3^-$. In addition to the constant area of the peak to which bromate contributes, chromatograms obtained in the presence of $TiO_2$ Wackherr and Degussa P25 show significant differences in the amount and presence of peaks related to the degradation intermediates. This finding is in general agreement with earlier suggestions that different photocatalysts induce not only different transformation kinetics, but also different degradation mechanisms.[13]
TOC measurements (Fig. 9) show that bromate slightly increased mineralization with $TiO_2$ Wackherr and slightly decreased it with Degussa P25. After 240 minutes of irradiation without $BrO_3^-$, the percentage of the residual organic compounds was reduced to 17% for $TiO_2$ Wackherr and to 4% for Degussa P25. In the presence of $BrO_3^-$, the corresponding values were 5% for $TiO_2$ Wackherr and 13% for Degussa P25. Photonic efficiencies of mineralization of MET after 60 min in the presence of $TiO_2$ Wackherr and Degussa P25 with $KBrO_3$ were 0.096%, and 0.194%, respectively.

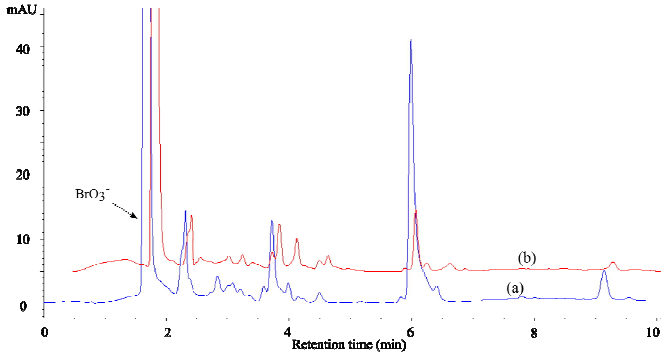


Fig. 8. Chromatograms obtained after 10 min of UV irradiation of MET in the presence of $TiO_2$ Wackherr (a) and Degussa P25 (b), in the $O_2/BrO_3^-$ system (3 mM bromate, $O_2$ bubbling); $\lambda_{det}$ = 225 nm

## 3.5. Influence of radicals on MET – DFT insight

### 3.5.1. Structural and reactivity properties - Fukui functions and indices

To better understand the interaction between MET and the radicals produced by reaction between $e^-$ and electron acceptors, we conducted a DFT computational analysis of the following systems: $MET/O_2^{\bullet-}$, $MET/O_2^{\bullet-}/^{\bullet}OH$, $MET/O_2^{\bullet-}/BrO_2^{\bullet}$, and $MET/O_2^{\bullet-}/SO_4^{\bullet-}$. The optimized molecular geometries of the investigated systems, together with the specific dihedral angles, are given in Fig. 10. The presence of $O_2^{\bullet-}$ (Fig. 10b) modifies dihedral angles, which reduces MET stability. Moreover, the interaction between $O_2^{\bullet-}$ and MET is modified by other electron acceptors (Fig. 10c-d).

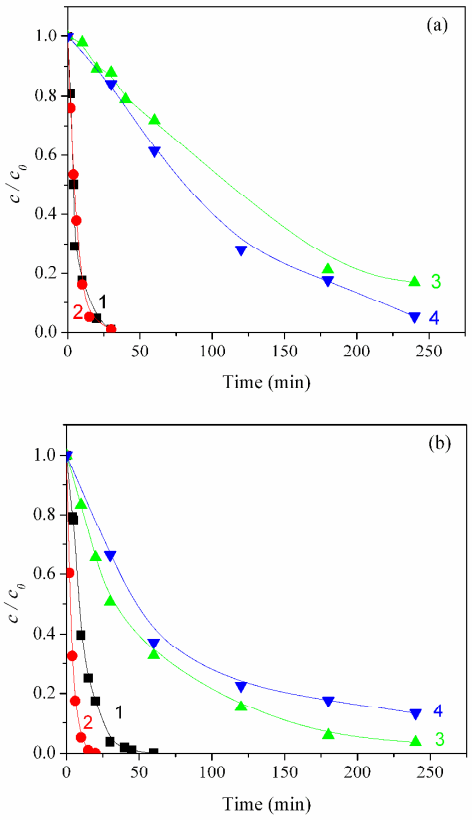


Fig. 9. Kinetics of photocatalytic degradation of MET under UV irradiation with $O_2$ bubbling, in the presence of $TiO_2$ Wackherr (a) and Degussa P25 (b): (1) MET trend, no $BrO_3^-$; (2) MET trend, 3 mM $BrO_3^-$; (3) TOC trend, no $BrO_3^-$; (4) TOC trend, 3 mM $BrO_3^-$.

The interaction distance between $O_2^{\bullet-}$ and MET was the shortest (1.612 Å) when $^{\bullet}OH$ was also present, while it was the longest (3.904 Å) in the presence of $SO_4^{\bullet-}$. Concerning other radicals, the interaction distance with MET was *ca*. 3.4 and 6.4 Å for $BrO_2^{\bullet}$ and $SO_4^{\bullet-}$, respectively. The most interesting situation for the interaction of radicals with MET was found in the case of $^{\bullet}OH$, where a new bond was formed. In various experimental studies carried out with molecules similar to MET, it was concluded that $^{\bullet}OH$ binds to the aromatic ring.[13,49] However, it was still unclear which carbon atom formed a bond with $^{\bullet}OH$. According to our study, a bond is formed with the carbon atom number 4 (Fig. 10).
Structural properties indicate that the highest interaction between MET and radicals takes place in the $MET/O_2^{\bullet-}/^{\bullet}OH$ system. These data are in overall agreement with the experimental results reported before, which emphasized the

important role of $O_2$ *vs*. deoxygenated systems and the effect of electron acceptors in the enhancement of $^{\bullet}OH$ (and $h^+$) occurrence, through inhibition of $e^-$–$h^+$ recombination. This fact is also confirmed by the NBO analysis provided in section 3.5.3 (*vide infra*).

In order to understand the reactive properties of MET, we will refer to Fukui functions and Fukui indices. Fukui functions are presented in Fig. 11, while Fukui indices ($f_{NN}$ HOMO and $f_{NN}$ LUMO) are given in Table 2. Fukui indices are commonly used since they describe the electron density when the molecule is subjected to a reaction that modifies the electron density itself.[50–52] Concerning the Fukui functions ($f^-$ and $f^+$), the red colour corresponds to the negative values while the blue colour corresponds to the positive ones. Negative values of $f^-$ correspond to regions that lose electron density when the molecule is subjected to electrophilic attack, or when the molecule itself acts as a nucleophile. Positive values of $f^+$ correspond to areas that gain electron density when the an molecule is subjected to nucleophilic attack, or when it acts as electrophile.

The $f_{NN}$ HOMO indices are related to the $f^-$ Fukui function, while the $f_{NN}$ LUMO ones are related to $f^+$. In other words, a high positive value of $f_{NN}$ HOMO indicates that the relevant atom can donate electrons, thereby acting as a nucleophile, while an elevated $f_{NN}$ LUMO indicates that the atom can receive electrons, thus acting as an electrophile. Having in mind the fact that a new bond was formed between MET and $^{\bullet}OH$, special attention was paid to the C4 atom of the MET aromatic ring, namely the atom involved in bond formation. According to positive surface of Fukui $f^+$ function, the MET molecule has an electrophilic nature on both tail parts. On the other hand, the negative value of $f^-$ located at the aromatic ring, and automatically at the C4 atom, suggests that this atom could act as a nucleophile as well. Significant values of both Fukui functions are located at the oxygen atom O7 (Fig. 11), while its Fukui indices emphasize nucleophilic nature (Table 2).

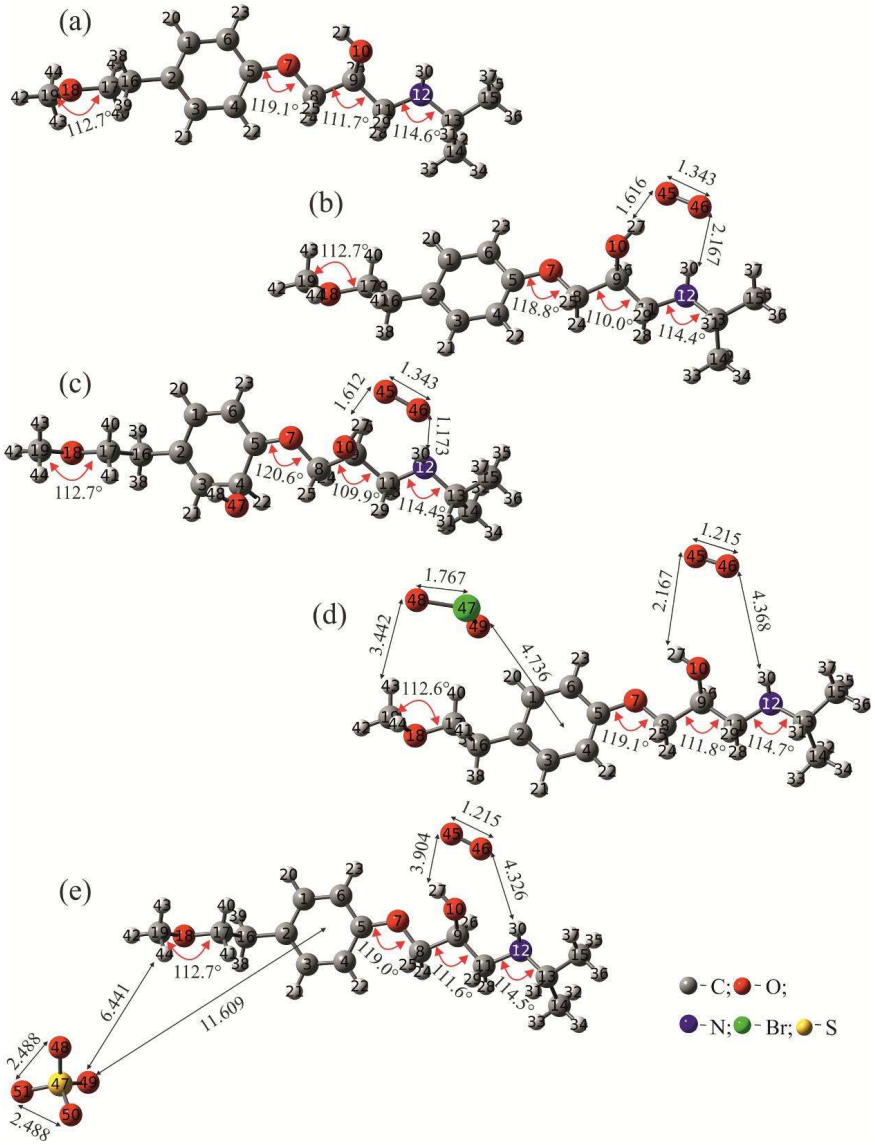


Fig. 10 Optimized geometries of the investigated structures with specific angles (degrees) and distances (Å) for: a) MET; b) MET/ $O_2^{\bullet-}$; c) MET/ $O_2^{\bullet-}$ /$^{\bullet}OH$; d) MET/ $O_2^{\bullet-}$ / $BrO_2^{\bullet}$; and e) MET/ $O_2^{\bullet-}$ / $SO_4^{\bullet-}$.

RSC Advances RSCPublishing

ARTICLE

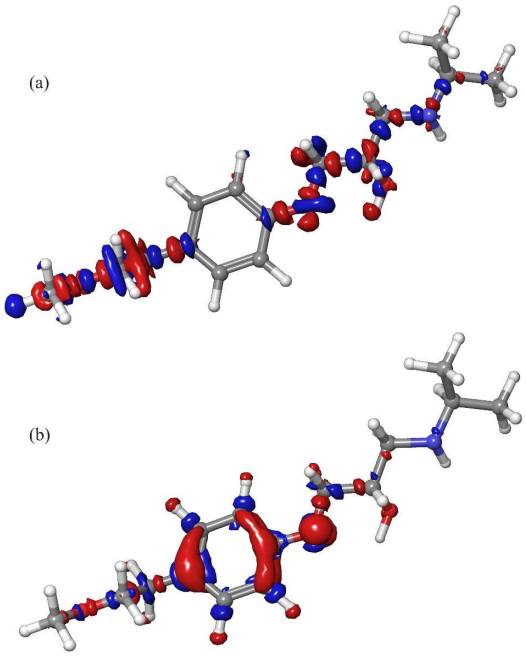


Fig. 11 Fukui functions of MET: a) Fukui $f^+$ function and b) Fukui $f^-$ function.

Table 2. Atomic Fukui indices of MET

| Atom | $f_{NN}$ HOMO | $f_{NN}$ LUMO |
|---|---|---|
| C1 | 0.0344 | 0.2021 |
| C2 | 0.2415 | 0.0115 |
| C3 | 0.0714 | 0.2885 |
| C4 | 0.1006 | 0.1777 |
| C5 | 0.1795 | 0.0070 |
| C6 | 0.1184 | 0.2969 |
| O7 | 0.1739 | 0.0006 |
| C8 | 0.0012 | 0.0014 |
| C9 | 0.0000 | 0.0048 |
| O10 | 0.0007 | -0.0026 |
| C11 | 0.0013 | 0.0011 |
| N12 | 0.0061 | -0.0008 |
| C13 | 0.0004 | 0.0002 |
| C14 | 0.0002 | 0.0001 |
| C15 | 0.0000 | 0.0001 |
| C16 | 0.0071 | 0.0016 |
| C17 | 0.0219 | -0.0035 |
| O18 | 0.0025 | 0.0004 |
| C19 | 0.0018 | 0.0004 |

Concerning Fukui indices, the value of $f_{NN}$ HOMO for the atom C4 again emphasizes its nucleophilic nature, while the highest value of this index is recorded for the C2 atom. The highest value of $f_{NN}$ LUMO is obtained for the atom C6. Overall, Fukui indices have significantly high values for atoms belonging to the aromatic ring.

One should be careful when interpreting the results of Fukui functions and indices, since they are not reliable to absolutely identify the most reactive electrophilic or nucleophilic sites within a particular molecule. In such a case, they can serve only as qualitative indicators of reactivity. However, according to both Fukui functions and indices, the C4 atom of the MET aromatic ring is a potential reaction site, which is confirmed in the case of the MET/ $O_2^{\bullet-}$ /$^{\bullet}$OH system.

### 3.5.2. Molecular Electrostatic Potential (MEP) surfaces

Representative MEP surfaces of the investigated structures are given in Fig. 12. The blue colour corresponds to the areas with the highest electrostatic potential, the red colour corresponds to the lowest electrostatic potential, while the green colour indicates intermediate values. MEP surfaces clearly indicate that significant changes of charge distribution would occur in MET in the presence of radicals. In particular, the introduction of radical species would change significantly the maximal and minimal MEP values, and the associated change would be the highest for $SO_4^{\bullet-}$. In the MEP surface of MET alone (Fig. 12) there are two specific sites containing a significant negative charge, located in the near vicinities of oxygen and nitrogen atoms. As expected, these sites would be the centres of reactivity with radicals. In the equilibrium state, $O_2^{\bullet-}$ was located above the hydroxyl group and the closest adjacent H atom. The hydroxyl radical was bound to the aromatic ring, and the H atom of $^{\bullet}$OH acquired a significantly positive MEP value. The situations changed when $BrO_2^{\bullet}$ and $SO_4^{\bullet-}$ were present in the system. The location of the radical $O_2^{\bullet-}$ was similar to previous cases, but the MEP values around $O_2^{\bullet-}$ were much higher than before and also the values around oxygen atoms increased significantly. These different charge distributions indicate interesting chemical interactions between MET and the studied radicals, which will be further discussed in the following section.

### 3.5.3. Natural Bond Order (NBO) analysis

The nature of molecular interactions can be investigated employing the NBO analysis, specifically based on the observation of the electron delocalization energies between NBO orbitals.[11,12,53–56] The significance of the chemical or physical interactions between MET and radical species can be assessed by using the total sum of the delocalization energies, $\Sigma E(2)$, obtained by summing the electron delocalization energies of all the significant interactions between the NBO orbitals of interacting molecules.[57,58] The $\Sigma E(2)$ values are reported in Table 3. A larger $\Sigma E(2)$ means that the interactions, resulting from electron delocalization from donor to acceptor NBO between MET and radicals, are more important. As a consequence, $\Sigma E(2)$ values are a measure of the importance of chemical interaction between the investigated species. On the other side, lower $\Sigma E(2)$ might suggest electrostatic interaction between the studied species.

RSC Advances

RSCPublishing

ARTICLE

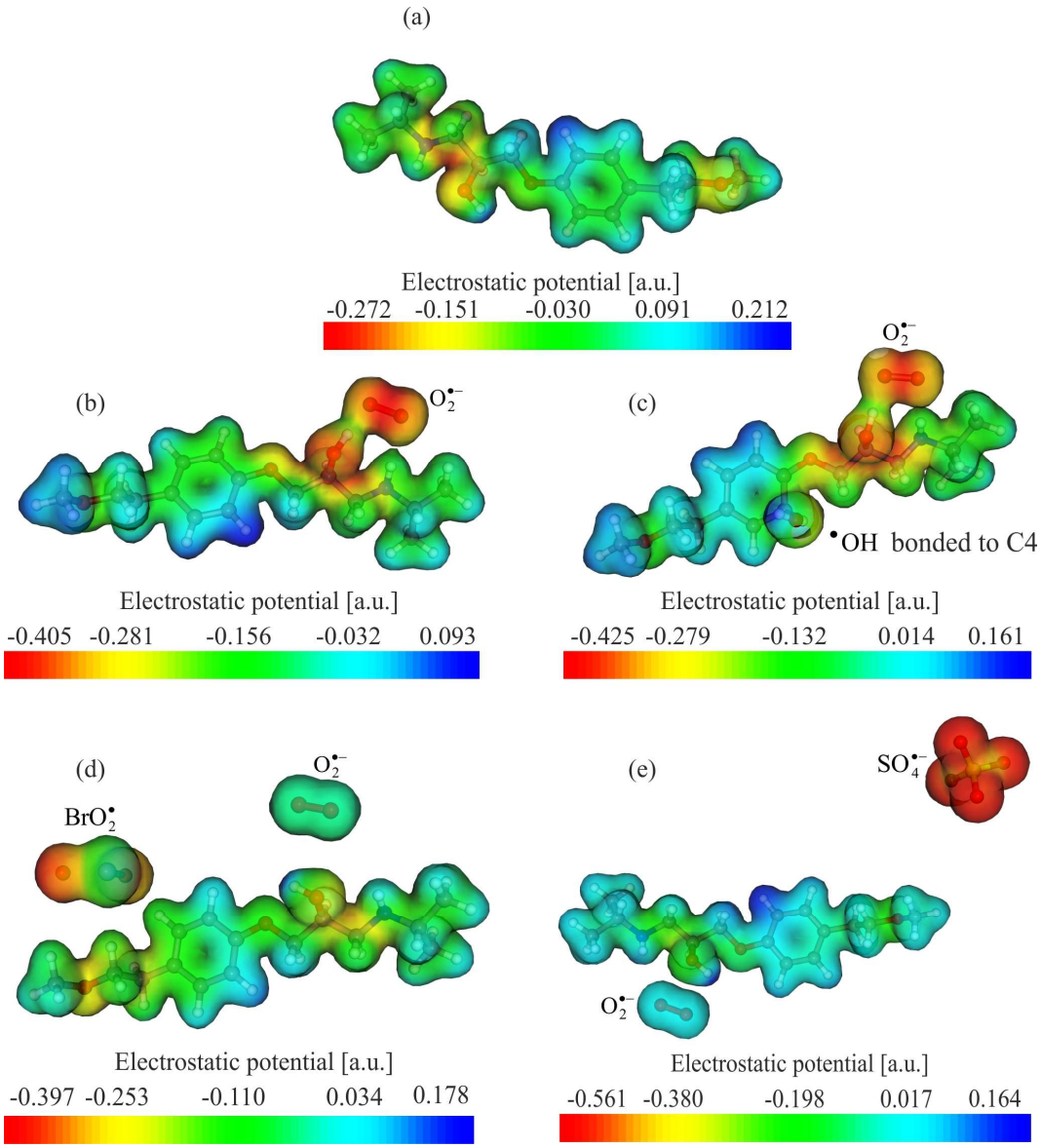


Fig. 12 Representative MEP surfaces of the investigated systems: a) MET; b) MET/ $O_2^{\bullet-}$; c) MET/ $O_2^{\bullet-}$ /$^{\bullet}$OH; d) MET/ $O_2^{\bullet-}$ / $BrO_2^{\bullet}$; and e) MET/ $O_2^{\bullet-}$ / $SO_4^{\bullet-}$.

According to NBO results, the highest and the most important chemical interactions took place in the MET/ $O_2^{\bullet-}$ /$^{\bullet}$OH system. This is consistent with above findings, which suggested that a new bond was formed in this system between the C4 atom of MET and $^{\bullet}$OH. The interactions resulting from electron delocalization from $O_2^{\bullet-}$ to MET NBOs are significant, since $\Sigma E(2) \approx 28$ kcal mol$^{-1}$. In contrast, chemical interactions resulting from electron delocalization from MET to $O_2^{\bullet-}$ NBOs are insignificant. There is a significant electron delocalization from $O_2^{\bullet-}$ to MET NBOs in the case of the MET/ $O_2^{\bullet-}$ system, as suggested by the quite elevated $\Sigma E(2) \approx 34$ kcal mol$^{-1}$. This is the highest value of $\Sigma E(2)$ among all the cases investigated in this work, and it clearly indicates a chemical interaction between $O_2^{\bullet-}$ and MET. This means that dissolved oxygen, in addition to inhibiting $e^-$–$h^+$ recombination and enhancing, as a consequence, the occurrence and subsequent reactivity of $^{\bullet}$OH and $h^+$, could further contribute to MET degradation through the formation of $O_2^{\bullet-}$.

Table 3. $\Sigma E(2)$ of interacting units between MET and radicals

| System | Donor unit (NBOs of) | Acceptor unit (NBOs of) | $\Sigma E(2)$ [kcal mol$^{-1}$] |
|---|---|---|---|
| MET/ $O_2^{\bullet-}$ | MET | $O_2^{\bullet-}$ | 3.14 |
| | $O_2^{\bullet-}$ | MET | 34.31 |
| MET/ $O_2^{\bullet-}$ /$^{\bullet}$OH | MET | $O_2^{\bullet-}$ | 0.23 |
| | MET | $^{\bullet}$OH | Bonded |
| | $^{\bullet}$OH | MET | Bonded |
| | $O_2^{\bullet-}$ | MET | 28.21 |
| | $O_2^{\bullet-}$ | $^{\bullet}$OH | <0.05 |
| | $^{\bullet}$OH | $O_2^{\bullet-}$ | <0.05 |
| MET/ $O_2^{\bullet-}$ / $BrO_2^{\bullet}$ | MET | $O_2^{\bullet-}$ | <0.05 |
| | MET | $BrO_2^{\bullet}$ | <0.05 |
| | $O_2^{\bullet-}$ | MET | 0.64 |
| | $BrO_2^{\bullet}$ | MET | 6.08 |
| | $O_2^{\bullet-}$ | $BrO_2^{\bullet}$ | <0.05 |
| | $BrO_2^{\bullet}$ | $O_2^{\bullet-}$ | <0.05 |
| MET/ $O_2^{\bullet-}$ / $SO_4^{\bullet-}$ | MET | $O_2^{\bullet-}$ | <0.05 |
| | MET | $SO_4^{\bullet-}$ | <0.05 |
| | $O_2^{\bullet-}$ | MET | <0.05 |
| | $SO_4^{\bullet-}$ | MET | <0.05 |
| | $O_2^{\bullet-}$ | $SO_4^{\bullet-}$ | <0.05 |
| | $SO_4^{\bullet-}$ | $O_2^{\bullet-}$ | <0.05 |

In the case of MET/ $O_2^{\bullet-}$ / $BrO_2^{\bullet}$, the $\Sigma E(2)$ of electron delocalization from $BrO_2^{\bullet}$ to MET NBOs is ca. 6 kcal mol$^{-1}$, which suggests weak chemical interaction when compared with previous cases. The chemical interaction between $O_2^{\bullet-}$ and MET in this system turned out to be insignificant, as indicated by a $\Sigma E(2)$ value from $O_2^{\bullet-}$ to MET of only 0.64 kcal mol$^{-1}$.

While important chemical reaction between MET and $BrO_2^{\bullet}$ seems to be excluded, it should be reminded that bromate was able to significantly enhance MET photocatalytic degradation in the case of Degussa P25. In this case, the effect of bromate should probably be ascribed to its mere ability to scavenge $e^-$, which inhibits the $e^-$–$h^+$ recombination and enhances the occurrence and subsequent reactivity of $^{\bullet}$OH and $h^+$. Moreover, the enhancement effect with Degussa P25 combined with no bromate effect on $TiO_2$ Wackherr suggests that an important role in MET degradation could be played by different properties of the photocatalyst, lifetime of $h^+$ and concentration of radical species.

In the case of MET/ $O_2^{\bullet-}$ / $SO_4^{\bullet-}$, the interactions between MET and the corresponding radicals would just be of an electrostatic nature, as suggested by the very low values of the $\Sigma E(2)$ energies, all below the default threshold of 0.05 kcal mol$^{-1}$. This result excludes chemical reactivity between MET and $SO_4^{\bullet-}$, and it helps explaining the very limited effect of $S_2O_8^{2-}$ on the photocatalytic degradation of MET. Indeed, electron scavenging by persulfate would be offset by drawbacks connected with $SO_4^{2-}$ formation (adsorption on the photocatalyst surface, which reduces the photocatalytic activity), while $SO_4^{\bullet-}$ would not be able to favour degradation by significantly reacting with MET.

### 3.6. LC–ESI–MS/MS identification of degradation intermediates

By using the LC–ESI–MS/MS technique, intermediates of MET degradation in the presence of different electron acceptors ($O_2$, $O_2/H_2O_2$ and $O_2/KBrO_3$) with both catalysts were investigated (see ESI,[§] Figs. S1-S22 and Table S1). Intermediates formed in the absence of electron acceptors (systems with $N_2$) were not investigated because the rate of MET degradation was very low. Therefore, the concentration of intermediates was low as well and they couldn't be identified. Because the collision-induced dissociation patterns of MET degradation were defined previously,[59] it was possible to identify the detected peaks by using the product ion $MS^2$ spectra. The retention times of all identified degradation intermediates **P1**–**P10** (1.18–3.98 min) were shorter than that of MET (4.43 min), due to the cleavage of the molecule and the formation of polar moieties.

During the degradation of MET with $TiO_2$ Wackherr/$O_2$, a total of seven peaks (labeled **P1–P7**) corresponding to degradation intermediates were detected (ESI,[§] Table S1 and Fig. 13). Intermediate **P1** represents a compound with $M_{mi}$ = 133, indicating the presence of a nitrogen atom in its structure. Based on its fragmentation pattern (ESI,[§] Table S1) and literature data, it was concluded that this compound is 3-(propan-2-ylamino)propane-1,2-diol, already identified.[13] Intermediates **P2** and **P3** both correspond to compounds with $M_{mi}$ = 253, but with different $MS^2$ spectra. Based on $MS^2$ spectra and literature data[13,60] it could be stated that **P2 is** hydroxy derivative 4-[2-hydroxy-3-(propan-2-ylamino) propoxy]benzaldehyde, that was previously identified as MET degradation product. Fragment 212 ($C_{10}H_{14}NO_4$) present in **P2**, is formed by loss of water and isopropyl moiety, which was further dehydrated to the *m/z* 177 (i.e., loss of water and methylamine group). Radjenović et al. also identified this compound and they stated that the characteristic fragment ion *m/z* 133 was detected in the spectrum of the parent compound and degradation products,[60] which is also in agreement with our results. The herewith provided $MS^2$ spectra of **P2** (Table S1) are in very good agreement with those previously reported.[13,60] It was not possible to determine the positions of the hydroxyls, due to the small number of fragments formed in $MS^2$ experiments. However, based on the theoretical results (Table 3 and Figs. 10 and 12), we can assume that $^{\bullet}$OH might be bonded to the C4 atom of the aromatic ring. Fragment 116 ($C_6H_{14}ON$), common to many MET degradation products, and observed in the $MS^2$ spectrum of **P3**, corresponds to *N*-(1-methylethyl)-2-oxopropan-1-aminium and indicates the intact *O*-bound moiety i.e. hydroxylation of either benzene ring or $C_2$-chain. Ion 177 fragments by consecutive loss of water (*m/z* = 18) and ethene (*m/z* = 28), indicating the presence of an hydroxyethyl moiety. The presence of ion 159 fragments in $MS^2$ spectra of MET and



 

**P3** indicates preserved aromatic ring of MET. Detailed fragmentation of MET is described in the literature, where *m/z* 159 corresponds to the loss of 109 (18+42+17+32) mass units: water, propene, ammonia are lost from the right side and methanol from the left side of the chain.[61] Thus, **P3** represents either 1-[4-(1-hydroxyethyl)phenoxy]-3-(propan-2-ylamino)propan-2-ol or its 2-hydroxyethyl isomer. This compound was previously identified[62,63] as the 1-hydroxyethyl isomer.

The three peaks, labelled **P4**, **P5,** and **P6**, corresponding to compounds with $M_{mi}$ = 281, were detected. Upon further evaluation of EICs for the observed fragment ions, it was determined that peak **P4** contains two closely-eluting compounds labelled **P4a** and **P4b**. Due to close elution, it was impossible to obtain pure $MS^2$ spectra of these compounds. Therefore, EIC traces for each ion had to be checked, to confirm the presence/absence of specific fragments in each chromatographic peak. To ease the comparison of spectra and interpretation, composite $MS^2$ spectra were prepared by summing $MS^2$ spectra obtained at different collision energies. Molecular mass, higher by 14 units than that of MET, implies the introduction of one oxygen and the abstraction of two hydrogen atoms (i.e. either introduction of an oxo group, or introduction of hydroxyl and oxidation of the existing hydroxyl). Early loss of isopropylamine and water ($\Delta m/z$ = 77, yielding fragment 205) and/or propene ($\Delta m/z$ = 42, yielding fragment 240) indicate the intact *i*PrNH–moiety. There are five possible isomers of oxo-MET (excluding the one with oxygenated isopropyl), hereby designated A–E. Isomer A: 2-{4-[2-hydroxy-3-(propan-2-ylamino)propoxy]phenyl}ethyl formate, isomer B: methyl {4-[2-hydroxy-3-(propan-2-ylamino)propoxy]phenyl}acetate, isomer C: 1-{4-[2-hydroxy-3-(propan-2-ylamino)propoxy]phenyl}-2-methoxyethanone, isomer D: 4-(2-methoxyethyl)phenyl-2-hydroxy-3-(propan-2-ylamino)propanoate, and isomer E: 2-hydroxy-3-[4-(2-methoxyethyl)phenoxy]-*N*-(propan-2-yl)propanamide. Based on differences in observed spectra, we tentatively assigned structures to detected peaks. The loss of $H_2O$ ($\Delta m/z$ = 18, yielding fragment 264), was observable only in peak **P6**, and was followed by subsequent loss of propylamine ($\Delta m/z$ = 59, yielding fragment 205). In all the other peaks the latter loss is immediate, and thus only ion 205 is observable, leading to the conclusion that ion 264 is stabilized in **P6**. Thus, we propose that **P6** represents either isomer D or E, that would – after water loss – form an α,β-unsaturated carbonyl compound, stabilized through electron delocalization. Peak **P5** was characterized by the absence of two otherwise common ions for MET and derivatives: 133 (corresponding to ion produced by loss of $H_2O$, *i*PrNH$_2$ and phenyl-bound chain) and 116 (corresponding to loss of *p*-substituted phenoxy moiety). Fragment 177, produced by loss of 28 mass units ($CO_2$/$C_2H_4$) from ion 205. We concluded that CO loss is to be expected if ion 205 has 1-formyl-2-[4-(2-methoxyethyl)phenoxy]ethenylium structure, i.e. if **P5** could represent the isomer E (in that case, **P6** would be the isomer D). The spectra of **P4a** and **P4b** differ from general pattern observed for **P5** and **P6** by much more pronounced fragments corresponding to loss of propene ($\Delta m/z$ = 42) or water and propylamine ($\Delta m/z$ = 77), and absence of otherwise common fragment 98 (either due to preferred loss of N-containing part as a neutral molecule, or due to low general abundance). Another common fragment, *m/z* 121, corresponding to protonated *p*-vinylphenol, was also absent in both peaks, which lead us to the conclusion that the oxidation possibly occurred at α- and β-position of 2-methoxyethyl moiety, i.e. that peaks **P4a** and **P4b** possibly represent isomers B and C. The presence of abundant fragment 116 (corresponding to intact *N*-(1-methylethyl)-2-oxopropan-1-aminium, formed by cleavage of phenoxy bond) seems to support the assumption. However, at the moment, it was not possible to determine the exact oxygenation site for these two compounds.

In the presence of $H_2O_2$ three new intermediates were observed (**P8**, **P9** and **P10**), while in the presence of $KBrO_3$ only **P9** and **P10** were detected. Intermediates **P7** and **P8** both have $M_{mi}$ = 299, which is by 32 mass units greater than for MET. This implies that they are dihydroxy MET derivatives.[13,49] Significant differences in fragmentation patterns of the two compounds allow the determination of the positions of the hydroxyl groups.

Intermediate **P7** was identified as 1-{4-[2-hydroxy-3-(propan-2-ylamino)propoxy]phenyl}-2-methoxyethane-1,2-diol. Initial loss of 62 mass units can be attributed to cleavage of the C-C bond between CHOH and CH(OH)$OCH_3$ units, leading to loss of methoxymethanol and formation of formyl group on benzene ring. Subsequent loss of propene ($\Delta m/z$ 42) leads to formation of ion 196. This ion further fragments by cleavage of the Ph-O bond, to yield two complementary ions at *m/z* 74 and 105.

Spectra of **P8** are dominated by a series of fragments characteristic for MET – 159, 133, 116, 74, 72 and 56. Since these ions correspond to preserved $C_2$-$C_6$-O-$C_3$-N moiety (without any additional substitution, compared to MET), we assume that the two hydroxyls are located at peripheral groups – methoxy and/or isopropyl. The value of *m/z* 282 corresponds to the parent compound after loss of water. However, it was not possible to determine where one or both hydroxyls are bound, due to the lack of any other diagnostic fragments. Intermediate **P9** has $M_{mi}$ = 273, namely six mass units higher than MET. This is a consequence of $C_3H_6$ loss and the attachment of three hydroxyl groups. However, at lower *m/z* range, a series of fragments was observed – 116 ($C_6H_{14}NO$), 98 ($C_6H_{12}N$), 74 ($C_3H_8NO$), 56 ($C_3H_6N$) – corresponding to *N*-(1-methylethyl)-2-oxopropan-1-aminium ion and its fragment, indicating a preserved 2-hydroxy-3-[(1-methylethyl)amino]propoxy group. Further fragmentation of ion 116 into 98 by the loss of water ($\Delta m/z$ =18) supports the presumption that the three hydroxyls are bonded to the methoxyethylbenzene moiety. The absence of common ions 159, 133 and 121 supports the oxidative cleavage of benzene ring, with the loss of a $C_2$ unit. While this reaction was previously described,[63] the hereby detected compound **P9** exhibit $MS^2$ spectra different from the published ones, indicating differences in the structure and suggesting that there are three OH groups bound to a benzene ring. This leads to the conclusion that the compound is a trihydroxy derivative of 1-amino-3-[4-(2-methoxyethyl)phenoxy]propan-2-ol.

Intermediate **P10**, eluting at 1.57 min, corresponds to a compound with $M_{mi}$ = 315. The short retention time suggests that it is very polar, which would be accounted for by the three hydroxyl groups present in its structure, since its molecular mass is 48 mass units higher than that of MET.[13] The fragments 116, 98, 74, and 56 in its $MS^2$ spectra indicate that the propanylaminopropane moiety stays intact, while the three hydroxyls are bonded to the methoxyethylbenzene part of the molecule. This compound has been previously identified as a trihydroxy derivative of 1-[4-(2-methoxyethyl)phenoxy]-3-(propan-2-ylamino)propan-2-ol.[13,49]

RSC Advances RSCPublishing

ARTICLE

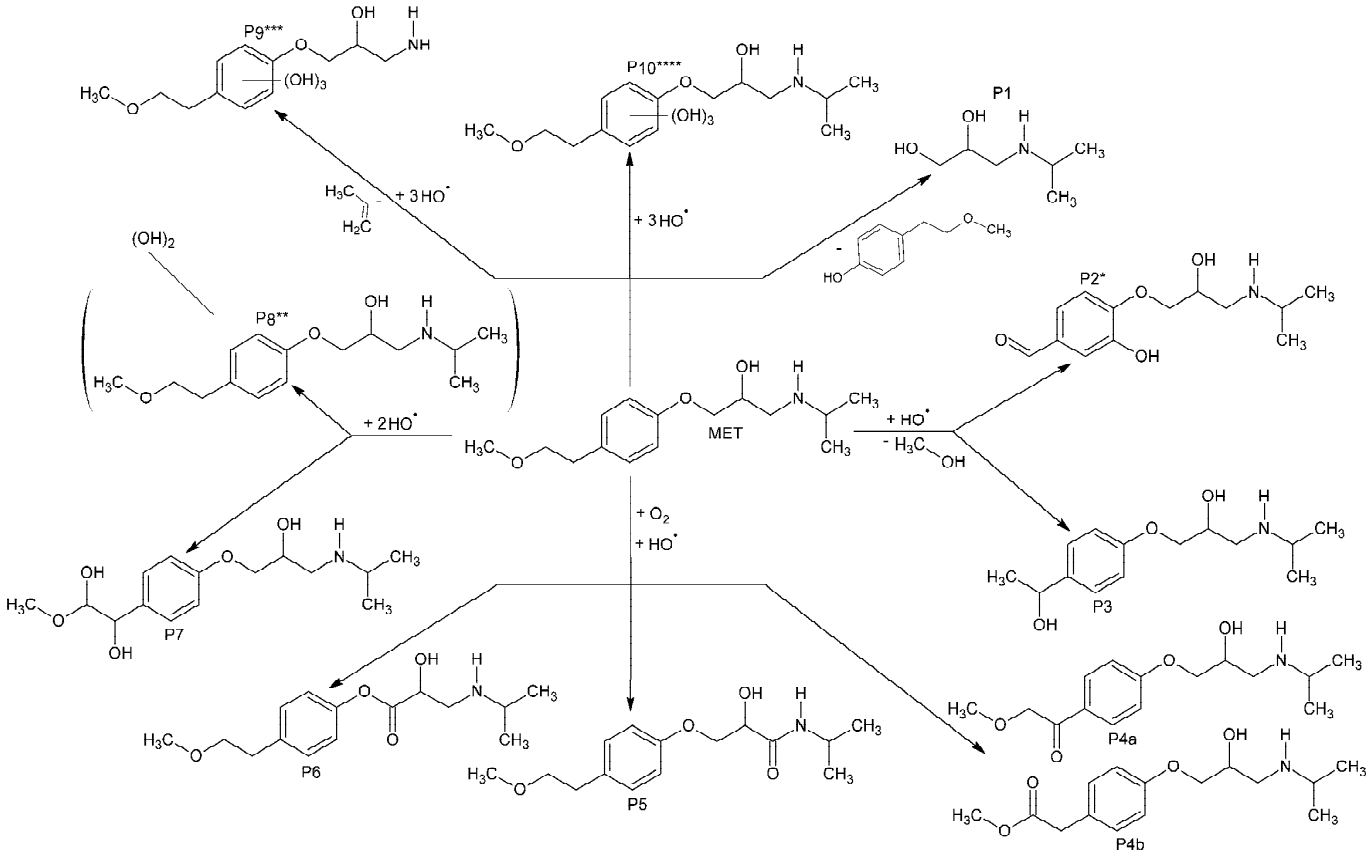


Fig. 13 Degradation intermediates of MET with electron acceptors, in the presence of $TiO_2$ Wackherr and Degussa P25. P1, P3–P7 were identified in all cases; P2* was identified, in all cases, only with $TiO_2$ Wackherr; P8** was identified only with $TiO_2$ Wackherr/$O_2$/$H_2O_2$; P9*** was identified in all cases except $TiO_2$ Wackherr/$O_2$; P10**** was identified in all cases except $TiO_2$ Wackherr/$O_2$ and Degussa P25/$O_2$/$KBrO_3$

The occurrence of different intermediates under different conditions could be due to their different stabilities, and/or to differences in the degradation mechanism of MET. One issue could be the interaction of $O_2^{\bullet-}$ with MET (Table 3). Compared to the case of $O_2$ alone, the addition of $H_2O_2$ lowered such interaction by 1.2 times and that of $KBrO_3$ by 54 times. However, NBO analysis already suggested that in the case of MET degradation with Degussa P25, besides the reactive radicals, the properties of the catalyst and the lifetime of $h^+$ would play an important role. This issue was confirmed by the analysis of the mechanism. Namely, in the presence of Degussa P25/$O_2$ the intermediates **P1**, **P3**–**P7**, **P9,** and **P10** were identified. Moreover, they were also identified in the presence of $H_2O_2$. This issue suggests that $H_2O_2$ in this case just increased the degradation rate of the parent compound (Fig. 1), which resulted in the faster formation of the intermediates because of an increased occurrence of $^{\bullet}OH$. The intermediate **P10** was not detected in the presence of $KBrO_3$, which might be due to the lower $^{\bullet}OH$ concentration in the system.

Similarly to our previous work, here it was confirmed that different sets of MET intermediates are formed with different photocatalysts.[13] Indeed, **P2** and **P8** were not detected in the presence of Degussa P25/$O_2$, while **P8**, **P9** and **P10** were not found with $TiO_2$ Wackherr/$O_2$. By comparing the $O_2$/$H_2O_2$ systems with Degussa P25, **P2** and **P8** were again not identified, while in the case of $TiO_2$ Wackherr all intermediates were identified. In the presence of $O_2$/$KBrO_3$ with Degussa P25 the intermediate **P10** was absent, while in the presence of $TiO_2$ Wackherr **P10** was present, but **P8** was absent.

In the present work, a lower number of intermediates was detected in comparison with previous work.[13] That is probably a consequence of the significantly lower concentration of MET (by 60 times) used in the present work, which prevented the formation of dimeric species. Moreover, the concentrations (peak areas) of some intermediates in this work were very low and thus their identification was not possible.

## 4. Conclusions

This study shows that $TiO_2$ is a very effective photocatalyst for MET degradation, in the presence of electron acceptors such as $O_2$, $H_2O_2$, and $BrO_3^-$. The effect of the investigated electron

acceptors depends on their initial concentration and on the nature of the photocatalyst. Moreover, while enhancing the transformation of MET (at least with Degussa P25), $H_2O_2$ decreased the rate of MET mineralization with both $TiO_2$ types. This contrasting effect might be accounted for by differences in reaction pathways ($h^+$ vs. $^{\bullet}OH$) induced by the photocatalysts with and without $H_2O_2$, as the $^{\bullet}OH$ pathway (enhanced by $H_2O_2$) possibly did not favour the mineralization of the substrate. The same phenomenon could also account for the higher degree of mineralization achieved, without $H_2O_2$, by Degussa P25 compared to $TiO_2$ Wackherr. The higher surface area of Degussa P25 could also be an issue, as it would decrease the probability of photocatalyst poisoning by the degradation intermediates.

DFT calculations and NBO analysis suggested that $^{\bullet}OH$ and possibly $O_2^{\bullet-}$ could undergo chemical reaction with MET. It is, therefore, suggested that dissolved oxygen would not only enhance $^{\bullet}OH/h^+$ reactivity by scavenging $e^-$ and, therefore, inhibiting $e^-$–$h^+$ recombination; oxygen could additionally favour MET degradation through the formation of $O_2^{\bullet-}$. In contrast, reaction between MET and $BrO_2^{\bullet}$ or $SO_4^{\bullet-}$ would be excluded. In the case of $SO_4^{\bullet-}$, the finding helps explaining the limited effect of $S_2O_8^{2-}$ on MET degradation: $e^-$ scavenging by $S_2O_8^{2-}$ would be largely offset by the formation of sulfate in addition to $SO_4^{\bullet-}$. While sulfate decreases the photocatalytic activity by adsorbing on the surface of $TiO_2$, $SO_4^{\bullet-}$ would not be able to take part in MET transformation.

Interestingly, both DFT calculations and the approach based on Fukui functions and Fukui indices consistently suggested that $^{\bullet}OH$ would react with the MET aromatic ring, and particularly with its C4 atom.

Experimental study by LC–ESI–MS/MS indicated bonding of OH groups to different parts of MET, while results of theoretical analysis obtained in this investigation indicated bonding of OH group to the aromatic ring. According to the theoretical results, bonding of OH group to the C4 atom of benzene ring of **P2** was suggested. It was shown experimentally that the binding of OH groups does not occur on the propanylaminopropane group chain (**P8**, **P9,** and **P10**) and that ring opening doesn't occur as well, which is also in agreement with theoretical analysis. Besides, intermediates that are peculiar for the systems containing $H_2O_2$ and $KBrO_3$ were identified as well. Namely, **P8**, **P9,** and **P10** were detected with $TiO_2$ Wackherr/$O_2$/$H_2O_2$ and **P9** and **P10** with $TiO_2$ Wackherr/$O_2$/$KBrO_3$. While the same intermediates were identified with Degussa P25/$O_2$ and Degussa P25/$O_2$/$H_2O_2$, the intermediate **P10** was not identified with Degussa P25/$O_2$/$KBrO_3$.

## Acknowledgements

The authors greatly appreciate the financial support from the Ministry of Education, Science and Technological Development of the Republic of Serbia (Project No. 172042).

## References

1. S. N. Frank and A. J. Bard, *The Journal of Physical Chemistry*, 1977, **81**, 1484-1488.
2. P. A. Brugger, P. Cuendet and M. Graetzel, *Journal of the American Chemical Society*, 1981, **103**, 2923-2927.
3. M. R. Hoffmann, S. T. Martin, W. Choi and D. W. Bahnemann, *Chemical Reviews*, 1995, **95**, 69-96.
4. A. Fujishima, T. N. Rao and D. A. Tryk, *Journal of Photochemistry and Photobiology C: Photochemistry Reviews*, 2000, **1**, 1-21.
5. S. Ahmed, M. Rasul, W. N. Martens, R. Brown and M. Hashib, *Water, Air & Soil Pollution*, 2011, **215**, 3-29.
6. S. Malato, P. Fernández-Ibáñez, M. Maldonado, J. Blanco and W. Gernjak, *Catalysis Today*, 2009, **147**, 1-59.
7. C. Karunakaran and R. Dhanalakshmi, *Solar Energy Materials and Solar Cells*, 2008, **92**, 588-593.
8. W. Liu, S. Chen, W. Zhao and S. Zhang, *Desalination*, 2009, **249**, 1288-1293.
9. N. Kashif and F. Ouyang, *Journal of Environmental Sciences*, 2009, **21**, 527-533.
10. M. Muruganandham and M. Swaminathan, *Dyes and Pigments*, 2006, **68**, 133-142.
11. N. N. Chipanina, N. F. Lazareva, T. N. Aksamentova, A. Y. Nikonov and B. A. Shainyan, *Organometallics*, 2014, **33**, 2641-2652.
12. S. Kheirjou, A. Fattahi and M. M. Hashemi, *Computational and Theoretical Chemistry*, 2014, **1036**, 51-60.
13. B. Abramović, S. Kler, D. Šojić, M. Laušević, T. Radović and D. Vione, *Journal of Hazardous Materials*, 2011, **198**, 123-132.
14. S. Armaković, S. J. Armaković, J. P. Šetrajčić and I. J. Šetrajčić, *Journal of Molecular Modeling*, 2012, **18**, 4491-4501.
15. R. G. Parr and W. Yang, *Journal of the American Chemical Society*, 1984, **106**, 4049-4050.
16. K. Chandrakumar and S. Pal, *International Journal of Molecular Sciences*, 2002, **3**, 324-337.
17. S. H. Rosline Sebastian Sr, M. I. Attia, M. S. Almutairi, A. A. El-Emam, C. Y. Panicker and C. Van Alsenoy, *Spectrochimica Acta Part A: Molecular and Biomolecular Spectroscopy*, 2014, **132**, 295-304.
18. S. Armaković, S. J. Armaković, J. P. Šetrajčić and I. J. Šetrajčić, *Chemical Physics Letters*, 2013, **578**, 156-161.
19. E. Kose, A. Atac, M. Karabacak, C. Karaca, M. Eskici and A. Karanfil, *Spectrochimica Acta Part A: Molecular and Biomolecular Spectroscopy*, 2012, **97**, 435-448.
20. M. Chen, U. Waghmare, C. Friend and E. Kaxiras, *The Journal of Chemical Physics*, 1998, **109**, 6854-6860.
21. A. J. Rossini, R. W. Mills, G. A. Briscoe, E. L. Norton, S. J. Geier, I. Hung, S. Zheng, J. Autschbach and R. W. Schurko, *Journal of the American Chemical Society*, 2009, **131**, 3317-3330.
22. J. Autschbach, S. Zheng and R. W. Schurko, *Concepts in Magnetic Resonance Part A*, 2010, **36**, 84-126.
23. R. J. Xavier and E. Gobinath, *Spectrochimica Acta Part A: Molecular and Biomolecular Spectroscopy*, 2012, **86**, 242-251.
24. M. Snehalatha, C. Ravikumar, I. Hubert Joe, N. Sekar and V. S. Jayakumar, *Spectrochimica Acta Part A: Molecular and Biomolecular Spectroscopy*, 2009, **72**, 654-662.
25. J. M. Dimitrić Marković, Z. S. Marković, J. B. Krstić, D. Milenković, B. Lučić and D. Amić, *Vibrational Spectroscopy*, 2013, **64**, 1-9.
26. Z. Marković, D. Milenković, J. Đorović, J. Dimitrić Marković, B. Lučić and D. Amić, *Monatshefte Fur Chemie*, 2013, **144**, 803-812.
27. S. F. Owen, E. Giltrow, D. B. Huggett, T. H. Hutchinson, J. Saye, M. J. Winter and J. P. Sumpter, *Aquatic Toxicology*, 2007, **82**, 145-162.
28. A. M. Stolker, W. Niesing, E. Hogendoorn, J. M. Versteegh, R. Fuchs and U. T. Brinkman, *Analytical and Bioanalitical Chemistry*, 2004, **378**, 955-963.
29. B. Kasprzyk-Hordern, R. M. Dinsdale and A. J. Guwy, *Water Research*, 2009, **43**, 363-380.
30. D. Bendz, N. A. Paxéus, T. R. Ginn and F. J. Loge, *Journal of Hazardous Materials*, 2005, **122**, 195-204.
31. S. Wiegel, A. Aulinger, R. Brockmeyer, H. Harms, J. Löffler, H. Reincke, R. Schmidt, B. Stachel, W. von Tümpling and A. Wanke, *Chemosphere*, 2004, **57**, 107-126.
32. D. Vione, C. Minero, V. Maurino, M. E. Carlotti, T. Picatonotto and E. Pelizzetti, *Applied Catalysis B: Environmental*, 2005, **58**, 79-88.
33. M. Frisch, G. Trucks, H. Schlegel, G. Scuseria, M. Robb, J. Cheeseman, J. Montgomery Jr, T. Vreven, K. Kudin and J. Burant, Gaussian.
34. A. D. Bochevarov, E. Harder, T. F. Hughes, J. R. Greenwood, D. A. Braden, D. M. Philipp, D. Rinaldo, M. D. Halls, J. Zhang and R. A. Friesner, *International Journal of Quantum Chemistry*, 2013, **113**, 2110-2142.

35. A. D. Becke, *The Journal of Chemical Physics*, 1993, **98**, 5648.
36. U. Varetto, *Swiss National Supercomputing Centre, Manno, Switzerland*, 2009.
37. G. V. Buxton, C. L. Greenstock, W. P. Helman and A. B. Ross, *Journal of Physical and Chemical Reference Data*, 1988, **17**, 513-886.
38. S. Chen and Y. Liu, *Chemosphere*, 2007, **67**, 1010-1017.
39. N. A. Mir, M. M. Haque, A. Khan, M. Muneer and C. Boxall, *The Scientific World Journal*, 2012, **2012**, 1-8.
40. W. Chu and C. Wong, *Water Research*, 2004, **38**, 1037-1043.
41. V. N. Despotović, B. F. Abramović, D. V. Šojić, S. J. Kler, M. B. Dalmacija, L. J. Bjelica and D. Z. Orčić, *Water, Air & Soil Pollution*, 2012, **223**, 3009-3020.
42. I. Poulios, M. Kositzi and A. Kouras, *Journal of Photochemistry and Photobiology A: Chemistry*, 1998, **115**, 175-183.
43. N. San, A. Hatipoğlu, G. Koçtürk and Z. Çınar, *Journal of Photochemistry and Photobiology A: Chemistry*, 2001, **139**, 225-232.
44. S. Qourzal, N. Barka, M. Tamimi, A. Assabbane and Y. Ait-Ichou, *Applied Catalysis A: General*, 2008, **334**, 386-393.
45. M. I. Stefan, A. R. Hoy and J. R. Bolton, *Environmental Science & Technology*, 1996, **30**, 2382-2390.
46. N. A. Mir, A. Khan, A. Dar and M. Muneer, *International Journal of Innovative Research in Science, Engineering and Technology*, 2014, **3**, 9333-9348.
47. D. D. Četojević-Simin, S. J. Armaković, D. V. Šojić and B. F. Abramović, *Science of The Total Environment*, 2013, **463**, 968-974.
48. D. V. Šojić, D. Z. Orčić, D. D. Četojević-Simin, V. N. Despotović and B. F. Abramović, *Journal of Molecular Catalysis A: Chemical*, 2014, **392**, 67-75.
49. H. Yang, T. An, G. Li, W. Song, W. J. Cooper, H. Luo and X. Guo, *Journal of Hazardous Materials*, 2010, **179**, 834-839.
50. E. Chamorro and P. Pérez, *The Journal of Chemical Physics*, 2005, **123**, 114107.
51. R. R. Contreras, P. Fuentealba, M. Galván and P. Pérez, *Chemical Physics Letters*, 1999, **304**, 405-413.
52. A. D. Bochevarov, E. Harder, T. F. Hughes, J. R. Greenwood, D. A. Braden, D. M. Philipp, D. Rinaldo, M. D. Halls, J. Zhang and R. A. Friesner, *International Journal of Quantum Chemistry*, 2013, **113**, 2110-2142.
53. S. Armaković, S. J. Armaković, J. P. Šetrajčić, S. K. Jaćimovski and V. Holodkov, *Journal of Molecular Modeling*, 2014, **20**, 1-14.
54. O. E. Kasende, A. Matondo, M. Muzomwe, J. T. Muya and S. Scheiner, *Computational and Theoretical Chemistry*, 2014, **1034**, 26-31.
55. D. Y. Buissonneaud, T. van Mourik and D. O'Hagan, *Tetrahedron*, 2010, **66**, 2196-2202.
56. S. Armaković, S. J. Armaković and J. P. Šetrajčić, *International Journal of Hydrogen Energy*, 2013, **38**, 12190-12198.
57. P. R. Olivato, J. M. Santos, B. Contieri, C. R. Cerqueira, D. N. Rodrigues, E. Vinhato, J. Zukerman-Schpector and M. D. Colle, *Molecules*, 2013, **18**, 7492-7509.
58. P. R. Olivato, J. M. M. Santos, C. R. Cerqueira Jr, E. Vinhato, J. Zukerman-Schpector, S. W. Ng, E. R. T. Tiekink and M. D. Colle, *Journal of Molecular Structure*, 2012, **1028**, 97-106.
59. R. M. Borkar, B. Raju, R. Srinivas, P. Patel and S. K. Shetty, *Biomedical Chromatography*, 2012, **26**, 720-736.
60. J. Radjenović, C. Sirtori, M. Petrović, D. Barceló and S. Malato, *Applied Catalysis B: Environmental,* 2009, **89**, 255-264.
61. C. Slegersa, A. Maquillea, V. Deriddera, E. Sonveauxb, J. H. Jiwanc and B.Tilquin, *Radiation Physics and Chemistry*, 2006, **75**, 977-989.
62. D. Šojić, V. Despotović, D. Orčić, E. Szabó, E. Arany, S. Armaković, E. Illés, K. Gajda-Schrantz, A. Dombi, T. Alapi, E. Sajben-Nagy, A. Palágyi, Cs. Vágvölgyi, L. Manczinger, L. Bjelica and B. Abramović, *Journal of Hydrology,* 2012, **472–473**, 314-327.
63. J. Benner and T. A. Ternes*, Environmental Science & Technology*, 2009, **43**, 5472-5480.



 

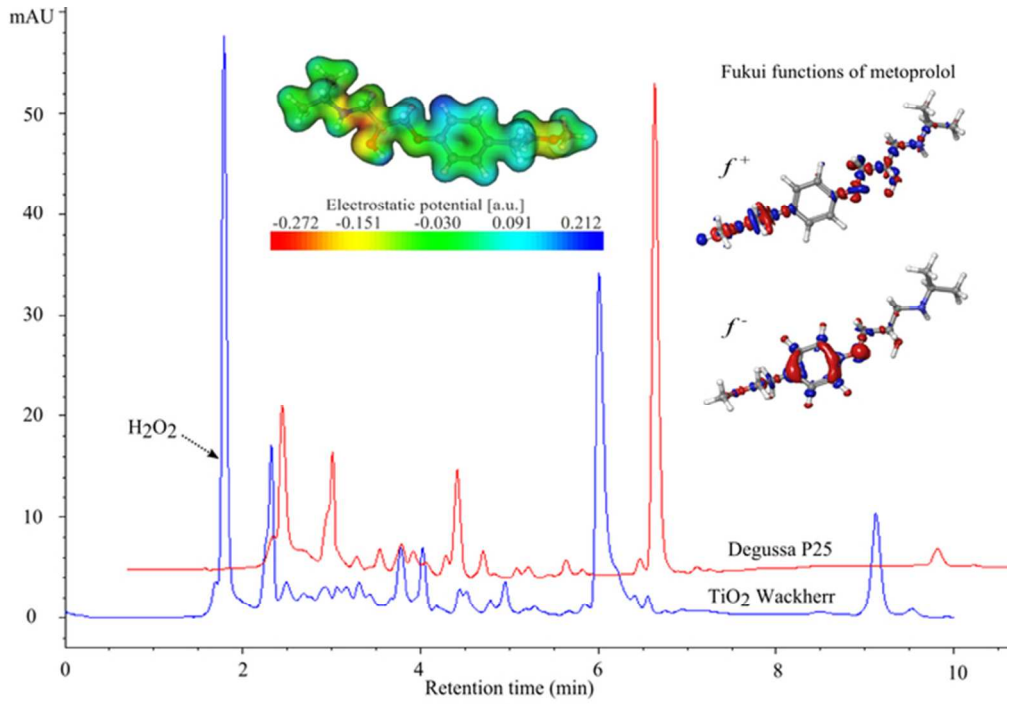


60x41mm (300 x 300 DPI)